Pergamon

PII: S0013-4686(96)00177-6

Electrochimica Acta, Vol. 42, No. 1, pp. 127–136, 1997

0013-4686/97 $17.00 + 0.00

Influence of *uv* light on the passive behaviour of SS316—effect of prior illumination

Carmel B. Breslin,* Digby D. Macdonald, Janusz Sikora and Elzbieta Sikora†

Center for Advanced Materials, The Pennsylvania State University, 517 Deike Building, University Park, PA 16802, U.S.A.

(Received 1 August 1995)

Abstract—The influence of *uv* light (300 nm) on the nucleation of meta-stable pits on type 316 stainless steel in a neutral 0.5 mol dm^{-3} NaCl solution using current–time measurements is described. A significant increase in the induction periods and a decrease in the rate of pit nucleation were observed for specimens pre-passivated under illumination conditions, indicating that illumination leads to a modification of the passive film that persists even after irradiation is removed. This increased resistance to pitting attack is explained in terms of the semiconducting nature of the passive film and the Point Defect Model (PDM) for the growth and breakdown of passive films. It is proposed that generation of electron–hole pairs leads to a quenching of the electric field strength and consequent modification of the vacancy structure, leading to a decrease in the flux of cation vacancies across the barrier layer. Good agreement was observed between the ratios of experimentally measured and theoretically calculated induction periods for specimens pre-passivated in the dark and in the light. Copyright © 1996 Elsevier Science Ltd

Key words: photo-inhibition, meta-stable pitting, SS316, *uv* light, passivity.

INTRODUCTION

The advent of photo-electrochemistry, which is now used successfully in probing the opto-electronic properties of passive films[1–6], has led to renewed interest in the phenomena of passivity and passivity breakdown. It has been shown that passive films on most metals and alloys exhibit semiconductive properties[1–6]. Also, there is ample evidence to suggest that the electronic properties of the passive film play a role in the breakdown mechanism. For example, Vijh[7] suggested that the corrosion potentials of several metals were correlated with the bandgap energies of the oxides. Sato[8], on comparing the corrosion behaviour of nickel and iron, concluded that *n*-type oxides were more resistant to passivity breakdown than *p*-type oxides. Burleigh and Latanision[9] and Menezes *et al.*[10] related the corrosion resistance of various alloys to the flat-band potentials. Burleigh[11], in a later study, proposed that anodic oxides were non-protective when in a degenerate state. The corrosion resistance of various stainless steels has also been related to the electronic properties of the passive film[12–14]. A relationship between the donor density and passive behaviour has been obtained[13], while scanning photo-current measurements have enabled the detection of potential breakdown sites[14].

Using the technique of photo-electrochemistry in a slightly different mode, it has been shown that illumination of certain materials with sufficiently energetic photons leads to a modification of the passive behaviour, which in turn results in an increased resistance to pitting attack[15–19]. This has been observed with pure nickel[15], iron[16, 17], SS316[18, 19], and SS304[19] in chloride-containing solutions.

In this communication, the influence of *uv* light (300 nm) on the passive behaviour and pitting susceptibility of SS316 in a 0.5 mol dm^{-3} NaCl solution is described. The results are discussed in terms of the semiconducting nature of the passive film and the Point Defect Model[20, 21] for the growth and breakdown of passive films.

*Permanent address: Department of Chemistry, St Patrick's College, Maynooth, Ireland.

†On leave from the Institute for Physical Chemistry, Polish Academy of Sciences, Warsaw, Poland.

EXPERIMENTAL

Test specimens were prepared from 316 (0.08% C, 2.0% Mn, 16.0% Cr, 12.0% Ni, 0.04% P, 0.03% S, 1.0% Si, 2.0% Mo) stainless steel rods, which were covered with lacquer, mounted in a PVC holder and then embedded in a two-component epoxy resin. The exposed surface, approximately 0.8 cm^2 in area, was polished mechanically with successively finer grades of SiC paper and finally to a mirror finish with 0.5 μm alumina powder. The surfaces were then cleaned ultrasonically with distilled water.

A three-electrode PTFE cell, equipped with a quartz window to allow irradiation of the test electrodes, was used as the test cell. A saturated calomel electrode (*sce*) was used as the reference electrode and a platinum wire, coiled inside the PTFE cell, was used as the auxiliary electrode. The test solutions, 0.5 mol dm^{-3} NaCl, were prepared from Analar-grade reagents and deionized water and were deoxygenated with nitrogen. The pH of the solutions was adjusted to 7.5 with NaOH. The working electrodes were irradiated at a wavelength of 300 nm and an incident power density of 0.4 mW cm^{-2} using a 150 W *uv*-enhanced Xe lamp (Oriel Model 6254) and a 1/8 m monochromator (Oriel Model 77250).

Electrochemical tests were carried out using a Solartron/Schlumberger Electrochemical Interface (Model 1286). In potentiodynamic polarization tests the working electrodes were polarized from the corrosion potential at a rate of 0.1 mV s^{-1} in the anodic direction up to the breakdown potential. In illumination experiments, the electrodes were illuminated continuously during the anodic scan. A total time of approximately 90 min was required for each experiment, thereby resulting in a total illumination period of 90 min. The breakdown potential was recorded when the current exceeded 80 μA cm^{-2}. In current–time studies and induction–time measurements, the electrodes were initially polarized at 0 V (*sce*) for a 90 min period, and then the potential was stepped to the desired value and the current was recorded as a function of time at a sampling rate of 90 ms using a Keithley Model 576 data acquisition unit. The induction period was deemed to be the interval between the application of this pre-selected potential and the onset of current fluctuations, which were indicative of meta-stable pitting. Exactly the same polarization periods were used for the illuminated and non-illuminated electrodes. However, in the illumination experiments, the surface was illuminated only for the first 90 min at 0 V (*sce*). The potential was then stepped to a pre-selected value, and the current–time transients were recorded in the dark. This ensured that a constant illumination period was facilitated in each experiment.

RESULTS AND DISCUSSION

Prior to discussing the experimental findings and presenting an explanation for them, it is first useful to define various potentials as they are used in this paper. Thus, the breakdown potential, E_b, is used to represent the potential at which pits have already initiated and are propagating to the extent that the current density reaches a value of 80 μA cm^{-2}. On the other hand, the critical breakdown potential, V_c, is the potential at which pits are first observed. Finally, the meta-stable pitting potential (V_{ms}) corresponds to the most negative potential at which current transients first appear and therefore approaches the critical breakdown potential (V_c). These three terms indicate the degree to which pitting is established and vary in the order $V_c < V_{ms} \ll E_b$.

The influence of light on the pitting susceptibility

The breakdown potentials of forty SS316 specimens were measured in a 0.5 mol dm^{-3} NaCl solution, twenty were polarized in the dark and twenty were polarized under conditions of illumination. The percentage cumulative probability[21] as a function of the breakdown potential was calculated for each set of data. The resulting plots, in which the cumulative probability is presented as a function of the breakdown potential, are shown in Fig. 1 for conditions of illumination and non-illumination. The data in each set agree with previous reports which have found that the breakdown potential is near-normally distributed[22]. It is clearly evident from these plots that illumination leads to a positive shift in the breakdown potential, the mean displacement in the breakdown potential, ΔE_b, being of the order of 60 mV.

The inhibition of pitting attack on illumination was evident also from induction–time measurements. SS316 specimens were polarized at 0 V (*sce*) under conditions of illumination and non-illumination for a 90 min period. Then the potential was stepped to +265, +235 or +220 mV (*sce*), and the current-transients were monitored under dark conditions; the light being switched off in the case of the illumination experiments ensuring a constant illumination period.

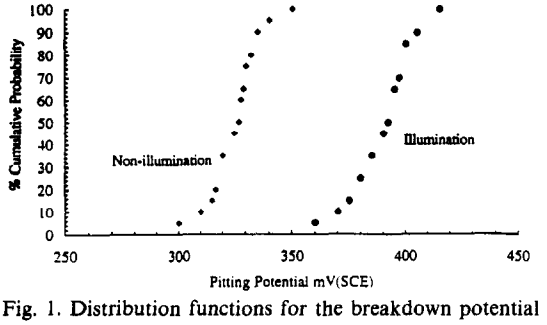

Fig. 1. Distribution functions for the breakdown potential measured for SS316 polarized in 0.5 mol dm^{-3} NaCl solution at a rate of 0.1 mV s^{-1} under conditions of illumination and non-illumination.

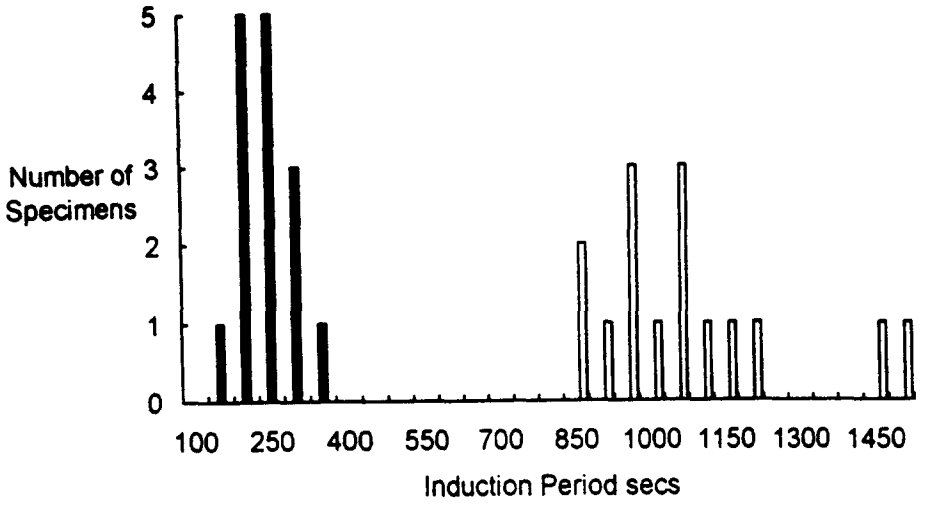

Fig. 2. Distribution of induction periods measured for SS316 polarized at +265 mV (*sce*) following a 90 min passivation period at 0 V (*sce*) in a neutral 0.5 mol dm^{-3} NaCl solution under conditions of illumination and non-illumination.

The induction periods were measured as the time intervals between the application of the second potential and the onset of current fluctuations (oscillations exceeding 500 nA). The induction periods measured for a total of thirty experiments, fifteen in the dark and fifteen in the light, at +265 mV (*sce*) are presented in Fig. 2, where the induction periods, divided into intervals, are plotted as a function of the number of experiments in which induction periods in the same interval were observed. Although some scatter was observed in these experiments, it is clear that illumination leads to a sizable increase in the induction period. This trend was observed with the three applied potentials selected; the average value of the induction periods in the dark at +235 mV (*sce*) was 930 ± 290 s, while in the light the value increased to 10,800 ± 3840 s. At the applied potential of +220 mV (*sce*), the average indiction period recorded in the dark was 4800 ± 1500 s, and that in the light was 72,000 ± 16,800 s. The fact that this initial 90 min illumination period has such a significant effect on the subsequent induction time for the nucleation of pits on the electrodes illustrates the persistence of the photo-inhibition effect, once the irradiation is removed.

It was found, also, that the frequency of meta-stable pitting events, after the elapse of the induction periods, was much reduced with prior illumination of the electrodes. This effect is shown by the representative plots in Figs 3 and 4, where the current–time transients on application of the final potentials of +265 mV (*sce*) and +235 mV (*sce*), respectively, are shown, both for conditions of prior illumination and non-illumination. It can be seen from these plots that a considerably smaller number of pits nucleate (reflected by the smaller number of current fluctuations) following illumination. Similar behaviour was observed at +220 mV (*sce*). These data, particularly those depicted in Fig. 4 for conditions of illumination, indicate that the pit-nucleation rate increases with increasing time, a finding that is quite different to that observed by Williams *et al.*[23]. A possible explanation for this difference is contained within the extended PDM[21], which accounts for the distributions in the breakdown voltage and induction time. Thus, assuming that the potential breakdown sites are normally-distributed with respect to the cation vacancy diffusivity, the nucleation rate (dN/dt) is predicted to increase with time at short times, but to become decreased with time at longer times. Thus, the nucleation rate apparently depends upon the point in the nucleation history at which it is observed. An alternative explanation may be found in the proposal by Pistorius and Burstein[24] that more aggressive conditions (as employed in this work compared with that of Williams *et al.*[23]) would result in a much higher population of potentially-active sites. This, in turn, would result in a much longer testing period for the exhaustion of these active sites, as only the sites that become activated and repassivated may be removed from the population[25].

It can be seen, from Figs 3 and 4, that prior illumination has little effect on the growth and decay of meta-stable pits. Indeed, it was found that continuous illumination, although modifying the frequency of the meta-stable pitting events, had no apparent effect on the lifetime of the meta-stable pits. This indicates that illumination modifies the passive film, but has little effect on any subsequent behaviour once breakdown of the passive film occurs.

An explanation for the photo-inhibition effect

The initial events that occur upon illumination of the immersed electrodes are easy to visualize. Provided the immersed electrodes are illuminated with light of a suitable energy, electrons are excited

from occupied (valence band or occupied states within the band) to unoccupied (conduction band) states to form electron–hole pairs or electron–ionized center pairs. Assuming that the electronic structure can be described by a Mott–Schottky barrier model and that a depletion layer exists within the film, the electron–hole pair become separated with the holes moving towards the surface.

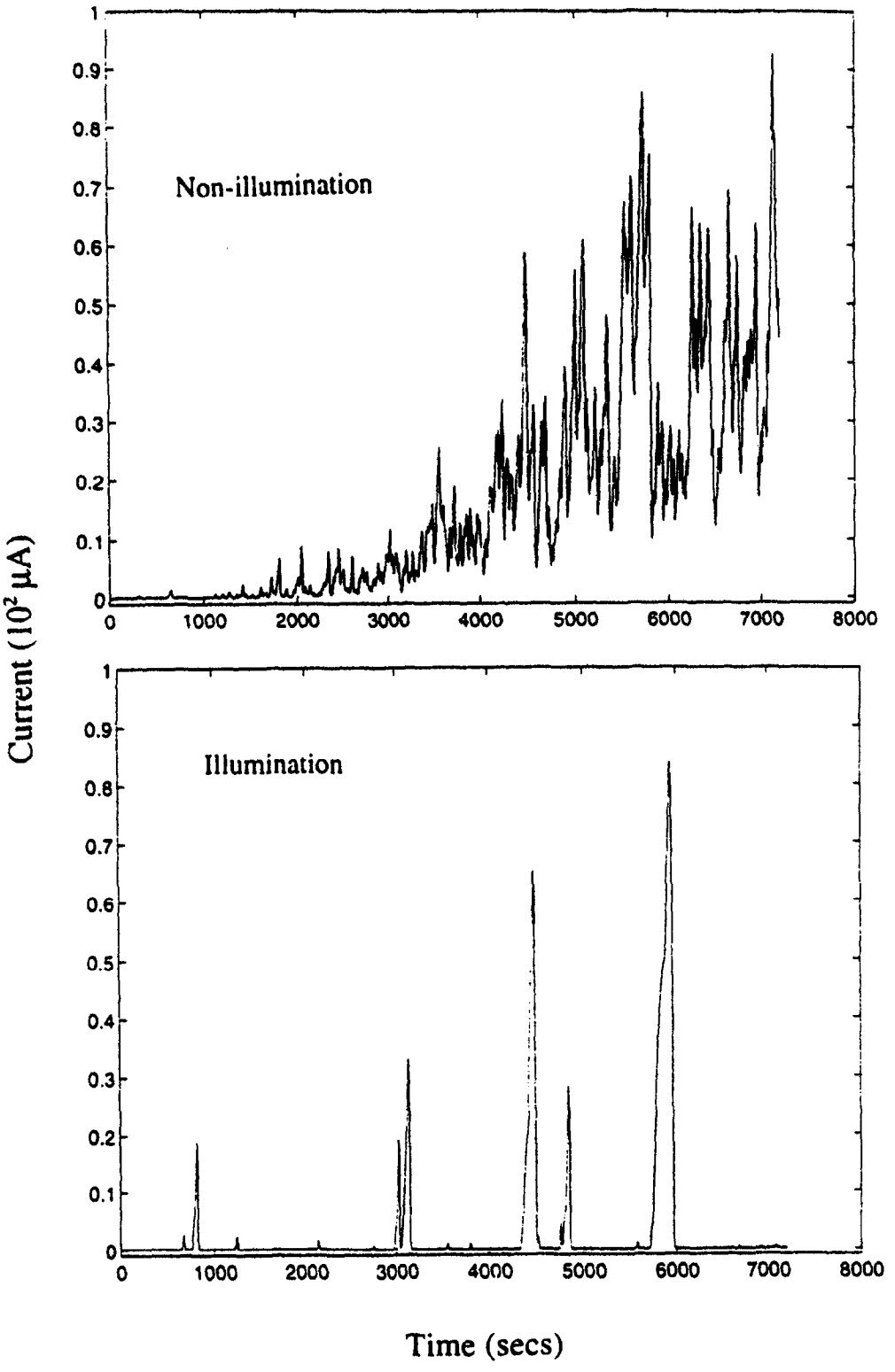

Fig. 3. Current–noise measurements for SS316 polarized at +265 mV (*sce*) (dark conditions) following a 90 min passivation period at 0 V (*sce*) in a neutral 0.5 mol dm^{-3} NaCl solution under conditions of non-illumination and illumination.

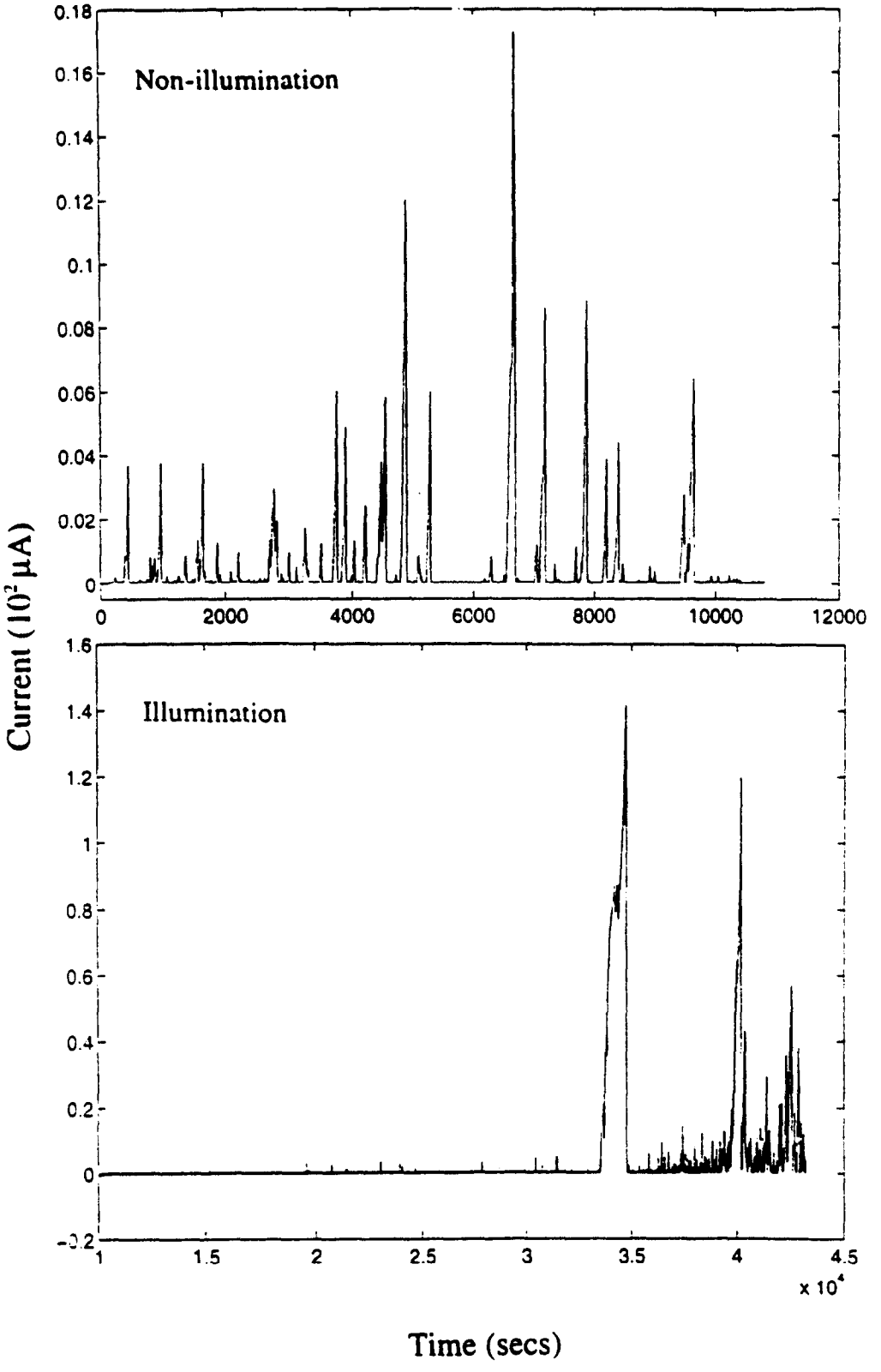

Fig. 4. Current–noise measurements for SS316 polarized at +235 mV (*sce*) (dark conditions) following a 90 min passivation period at 0 V (*sce*) in a neutral 0.5 mol dm^{-3} NaCl solution under conditions of non-illumination and illumination.

Photo-induced reactions involving the holes can occur at the film–solution interface, but it seems improbable that these are responsible for the observed photo-inhibition effect, because light should facilitate rather than inhibit localized dissolution, particularly because the passive film on stainless steels has been reported to be *n*-type[26] and because manganese sulfide is *p*-type (although the semiconductor character of MnS may change with Cr-doping). Thus, there appears to be little evidence to favour a sulfide inclusion dissolution mechanism, although photo-induced dissolution of sulfide inclusions may occur on illumination at very much higher intensities to induce pitting attack[26]. An increase in the film thickness is unlikely as Schmuki and Bohni[16, 17] found no change in the film thickness of pure iron on illumination with a much higher intensity of irradiation. However, light-induced film growth has been observed in the case of anodic oxide films on zirconium[27], with the extent of film growth being small but nevertheless consistent with the predictions of the PDM. It is also difficult to identify a photo-induced reaction, in a simple chloride solution, that could increase the resistance to pitting attack but not modify the thickness of the passive film. However, the separation of charge (*via* the photo-generation of electron–hole pairs) gives rise to a counter field, so that the electric field strength within the barrier layer is quenched. This situation will only persist while the electrode is illuminated, but, it is very likely that this process leads to a modification of the vacancy structure which is much slower to relax[18, 21]. This seems to be the most reasonable explanation, which in conjunction with the PDM can account for the observed photo-inhibition effect, as outlined below.

According to the PDM, passivity breakdown occurs as a result of the build-up of a critical concentration of cation vacancies at the metal–film interface which induces mechanical instability and rupture of the passive film. These ideas may be assembled[20] to derive expressions for the critical breakdown potential and induction period for a single breakdown site as,

$$V_c = \frac{4.606RT}{\chi F\alpha}\log\left(\frac{J_m}{J^0 u^{-\chi/2}}\right) - \frac{2.303RT}{\alpha F}\log(a_{x^-}) \quad (1)$$

and

$$t_{ind} = \xi'\left(\exp\left(\frac{\chi\alpha F\Delta V}{2RT}\right) - 1\right)^{-1} + \tau \quad (2)$$

respectively, where V_c is the critical breakdown potential, a_{x^-} is the activity of the aggressive anion in the solution, t_{ind} is the induction period, $\Delta V = V_{app} - V_c$, where V_{app} is the applied potential, χ is the oxide stoichiometry ($MO_{\chi/2}$), α is the dependence of the potential difference across the film–solution interface on the applied potential, J_m is the rate of annihilation of cation vacancies at the metal–film interface, J^0 is the flux of cation vacancies across the barrier layer, and ξ is the critical concentration of cation vacancies at the metal–film interface required to induce breakdown, and is related to ξ' through equation (3):

$$\xi' = \frac{\xi}{J^0 u^{-\chi/2}(a_{x^-})^{\chi/2}\exp\left(\frac{\chi\alpha FV_c}{2RT}\right)}. \quad (3)$$

The parameter τ was initially identified as a "relaxation time" but has since been identified as the time of dissolution of the cap above the cation vacancy condensate to the extent required for mechanical instability and hence rupture[21, 28]. For the thin passive films that form on iron and stainless steels, τ is likely to be of the order of seconds or tens of seconds. The parameter J^0 varies with the electric field strength (ϵ) in accordance with equation (4).

$$J^0 = \chi\frac{\epsilon F}{RT}D\left(\frac{Nv}{\Omega}\right)^{1+\chi/2} \times \exp\left(\frac{-\Delta G_s^0}{RT}\right) \quad (4)$$

where D is the cation vacancy diffusivity, Nv is Avagadro's constant, Ω is the molar volume of the oxide per cation, and ΔG_s^0 is the standard Gibbs energy of formation of cation–anion vacancy pairs at the film–solution interface. The parameter u in equation (3) may be expressed by equation (5):

$$u = \left(\frac{Nv}{\Omega}\right) \times \exp\left(\frac{-\Delta G_{A^-}^0 - \beta F\mathrm{pH} - F\phi_{f/s}^0}{RT}\right) \quad (5)$$

where $\Delta G_{A^-}^0$ is the standard Gibbs energy of absorption of an aggressive anion into an oxygen vacancy at the film–solution interface, β is the dependence of $\phi_{f/s}$ on pH, and $\phi_{f/s}^0$ is a constant.

It may be seen on combining equations (1) and (4) and equations (2), (3), and (4) that a decrease in the electric field strength gives rise to higher breakdown potentials and longer induction periods, in agreement with the data presented in Figs 1–4. It is proposed that a modification of the vacancy structure also occurs as a consequence of a decrease in the electric field strength, so that equating the persistent increased resistance to pitting with a quenching of the electric field strength is justified.

Analysis of the induction periods measured at the three applied potentials was carried out in order to test the agreement between the experimentally-obtained data and the predictions of the PDM. Using equations (2) and (3) to express the induction period measured for samples passivated in the dark and in the light, the ratio of the induction periods, $t_{ind}(\mathrm{light})/t_{ind}(\mathrm{dark})$, may be expressed by equation (6), where the subscripts d and l refer to dark and light conditions respectively.

$$\frac{t^{l}_{ind}}{t^{d}_{ind}} = \frac{\epsilon^{d}}{\epsilon^{l}} \times \frac{D_{d}}{D_{l}} \times \frac{\mu_{d}^{-\chi/2}}{\mu_{l}^{-\chi/2}} \times \frac{\exp\left(\frac{-\Delta G^{0}_{s}}{RT}\right)_{d}}{\exp\left(\frac{-\Delta G^{0}_{s}}{RT}\right)_{l}} \times \exp\left(\frac{\chi\alpha F}{2RT}(V^{d}_{c} - V^{l}_{c})\right) \times \left[\frac{\exp\left(\frac{\chi\alpha F}{2RT}(V_{app} - V^{d}_{c})\right) - 1}{\exp\left(\frac{\chi\alpha F}{2RT}(V_{app} - V^{l}_{c})\right) - 1}\right] \quad (6)$$

Assuming that the Gibbs free energies, ΔG^{0}_{s}, ΔG^{0}_{A-1}, and the cation vacancy diffusivity, D, are independent of illumination, then equation (6) may be simplified and reduced to equation (7).

$$\frac{t^{l}_{ind}}{t^{d}_{ind}} = \frac{\epsilon^{d}}{\epsilon^{l}} \times \left[\frac{1 - \exp\left(\frac{-\chi\alpha F}{2RT}(V_{app} - V^{d}_{c})\right)}{1 - \exp\left(\frac{-\chi\alpha F}{2RT}(V_{app} - V^{l}_{c})\right)}\right] \quad (7)$$

It can be seen from equation (7) that the experimental parameters are V^{d}_{c}, the critical breakdown potential for samples passivated in the dark, V^{l}_{c}, the critical breakdown potential for samples passivated in the light, V_{app}, and α.

The term α may be calculated from experimental data using equation (1), when the breakdown potential is expressed as a function of the logarithm of the chloride concentration. Experimental data plotted in this form are shown in Fig. 5 for conditions of illumination and non-illumination. The data points shown in this plot are the average of several experiments, and have uncertainties of about ± 20 mV. Although the breakdown potentials measured in this manner, using potentiodynamic methods, are clearly not critical breakdown potentials, it may be assumed that the difference between these measured breakdown potentials and the critical breakdown potentials is essentially constant over the chloride concentration range, and so the true value for α may be calculated from the slopes of these lines. An α value of 0.7 ± 0.1 was calculated for the two sets of data, indicating that α is independent of illumination. The insensitivity of α to illumination is consistent with photo-generated holes not being directly involved in the breakdown process.

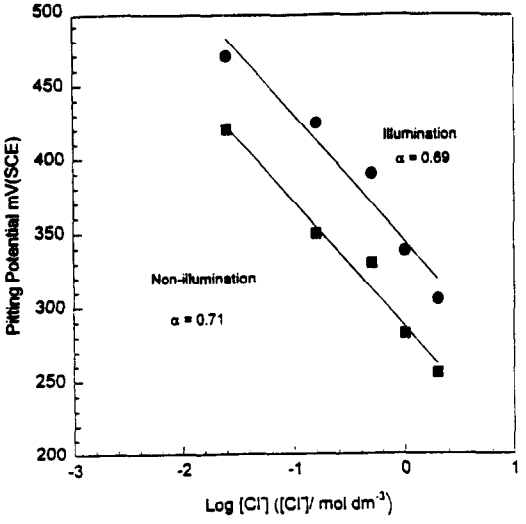

Fig. 5. Breakdown potential data for SS316 plotted as a function of the logarithm of the chloride anion concentration for conditions of illumination and non-illumination. Calculated α values shown.

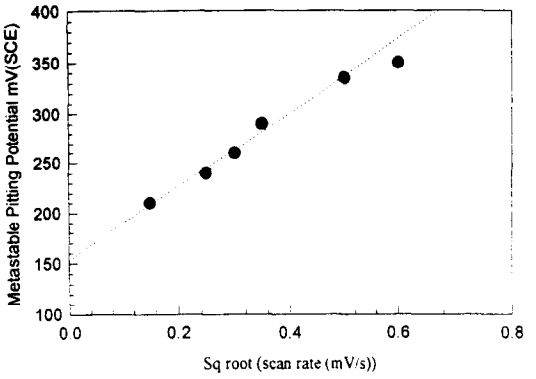

Fig. 6. Meta-stable breakdown potential data measured for SS316 in 0.5 mol dm^{-3} NaCl solution plotted as a function of the square root of the scan rate.

Values for the critical breakdown potentials were estimated from long-term potentiostatic experiments and measurements of the meta-stable breakdown potential as a function of scan rate. The meta-stable breakdown potential was measured as the potential at which the first current fluctuations (fluctuations in the nA range) were observed, on polarizing the specimens in the anodic direction. These meta-stable breakdown potential data, when plotted as a function of the square root of the scan rate gave a straight-line relationship (as predicted by the PDM[29]), which on extrapolation to zero scan rate yields a value of 150 ± 20 mV (*sce*) for the critical breakdown potential for specimens polarized in the dark in a 0.5 mol dm^{-3} NaCl solution (Fig. 6). In long-term potentiostatic experiments, the electrodes were polarized at a certain potential, and the current was monitored. If meta-stable pitting events were observed, then the polarizing potential was considered to be anodic to the critical breakdown potential. If no fluctuations were observed after the elapse of a 56 h period, then the polarizing potential was considered to be cathodic to the critical breakdown potential. An average value of 170 ± 20 mV (*sce*) was obtained for the critical breakdown potential using this method. It was not

possible to obtain the corresponding meta-stable breakdown potential for the illuminated specimens using these approaches, as variations in the illumination period leads to varying degrees of photo-inhibition[18]. Rather a potential of (60 ± 10) mV was added to the value of +150 mV (*sce*) calculated for dark conditions; 60 mV being the approximate displacement, ΔE_b, in the breakdown potential following a 90-min illumination period, as evident from Fig. 1. However, these values are subject to considerable uncertainty arising from uncertainties in the critical breakdown potentials and in the degree of photo-inhibition from specimen to specimen.

Using the experimental value of α, the critical breakdown values in the dark and in the light, and the change in the electric field strength upon illumination, the ratios of the induction periods in the light to those in the dark were calculated using equation (7). The decrease in the electric field strength was calculated using equation (8), which may be derived using equation (1) and by assuming that the standard Gibbs Free energies of processes that occur at the film–solution interface, and the cation vacancy diffusivities remain constant and hence independent of illumination.

$$\frac{\epsilon^l}{\epsilon^d} = \exp\left(\frac{\chi\alpha F}{2RT}(V_c^d - V_c^l)\right). \tag{8}$$

An applied potential of +265 mV (*sce*) was used in these calculations allowing a comparison with the experimental data collected at this potential. The results of these calculations are shown in Table 1, where the critical breakdown potential in the dark is allowed to vary from +150 to +140 mV (*sce*) and the displacement in the critical breakdown potential, ΔE_b, on illumination is varied between 50 and 70 mV. The decrease in the electric field strength is also shown.

The predicted induction-time ratios, shown in the right-hand column of the table, vary between 8 and 20. These data may be compared with the average value of 5 calculated from the experimental data (the induction period for specimens passivated in the dark being 237 ± 68 s, while that for specimens pre-passivated in the light being 1080 ± 205 s). When the degree of scatter in the experimental data is considered (Fig. 2), the fit between the experimental data and the theoretical calculations is probably as good as could be expected. This is more clearly evident from the data presented in Fig. 7, which show the experimentally-calculated ratios, t_{ind}(light)/t_{ind}(dark), as a function of the frequency of these ratios, for specimens polarized at a final potential of +265 mV (*sce*). These data were calculated by taking each induction period measured for specimens passivated in the light and in the dark (Fig. 2) and calculating all possible ratios. It is seen, from this figure, that ratios as high as 9 are observed experimentally.

Table 1
A comparison of the induction time ratios, t_{ind}^l/t_{ind}^d, calculated from the Point Defect Model and measured experimentally at an applied potential of +265 mV (*sce*)[a]

V_c^d (mV)	V_c^l (mV)	ΔE_b (mV)	$\frac{\epsilon^d}{\epsilon^l}$	$\frac{t_{ind}^l}{t_{ind}^d}$
+150	+200	50	7.7	8.2
	+210	60	11.6	12.9
+140	+190	50	7.7	8.1
	+200	60	11.6	12.4
	+210	70	17	19.4

[a]The following values were used in the calculations: $\alpha = 0.7$, measured from experimental data, Fig. 5; $\Delta E_b = (60 \pm 40)$ mV, measured from experimental data, Fig. 1; V_c^d varied from 150 mV to 140 mV. Experimental values of t_{ind}^l/t_{ind}^d are shown in Fig. 7.

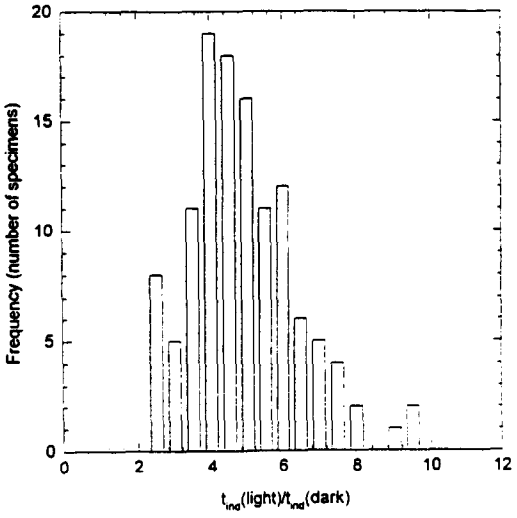

Fig. 7. Experimentally obtained ratios of the induction times for specimens passivated in the light and in the dark, t_{ind}^l/t_{ind}^d. Induction periods measured for SS316 polarized at +265 mV (*sce*) in 0.5 mol dm^{-3} NaCl solution, following a passivation period of 90 min at 0 V (*sce*) under conditions of illumination and non-illumination.

In Table 2, the ratios between the induction periods measured for specimens passivated in the light and in the dark at the three selected potentials are compared with the calculated ratios at the same potentials. In this case, α is allowed to vary in the calculations. Again acceptable agreement between the experimental observations and the calculated data is obtained. These experimental data are shown in graphical form in Fig. 8, with the ratio of the induction periods, t_{ind}(light)/t_{ind}(dark), plotted as a function of the applied potential. Shown also in these plots are calculated data in which the displacement in the breakdown potential on illumination is allowed to vary from 40 to 60 mV with the critical breakdown potential value set at 150 mV (*sce*). Given the fact that these variations in V_c and ΔE_b occur from experiment to experiment, it is clear that the experimental data fall well within the bands

Table 2
A comparison of the induction time ratios, t^l_{ind}/t^d_{ind}, calculated from the Point Defect Model and measured experimentally as a function of the applied potential, V_{app}, in a 0.5 mol dm^{-3} NaCl solution[a]

V_{app} (mV (*sce*))	t_{ind} (dark) average (s)	t_{ind} (dark) average (s)	t^l_{ind}/t^d_{ind} (exp.)	α	t^l_{ind}/t^d_{ind} (calc.)
+ 265	237	1080	4.6	0.7	12.9
				0.6	9.4
				0.8	17.8
+ 235	930	10,800	11.6	0.7	17.6
				0.6	13.3
				0.8	23.5
+ 220	4800	72,000	15.0	0.7	32.6
				0.6	25.3
				0.8	42.5

[a]The following values were used in the calculations: $V^d_c = 150$ mV; $\Delta E_b = 60$ mV measured from experimental data (Fig. 1); α was allowed to vary between 0.6 and 0.8.

calculated from the PDM. It is also evident that, for polarizing conditions close to the critical pitting potentials (lower applied potentials), very large differences between the induction periods for dark and light conditions are predicted. This is important with respect to the pitting corrosion of stainless steels under natural immersion conditions where, for conditions when the corrosion potential is close to the breakdown potential, illumination of the electrodes is predicted to increase significantly the induction period.

It is seen from this analysis that the photoinhibition effect may be explained within the

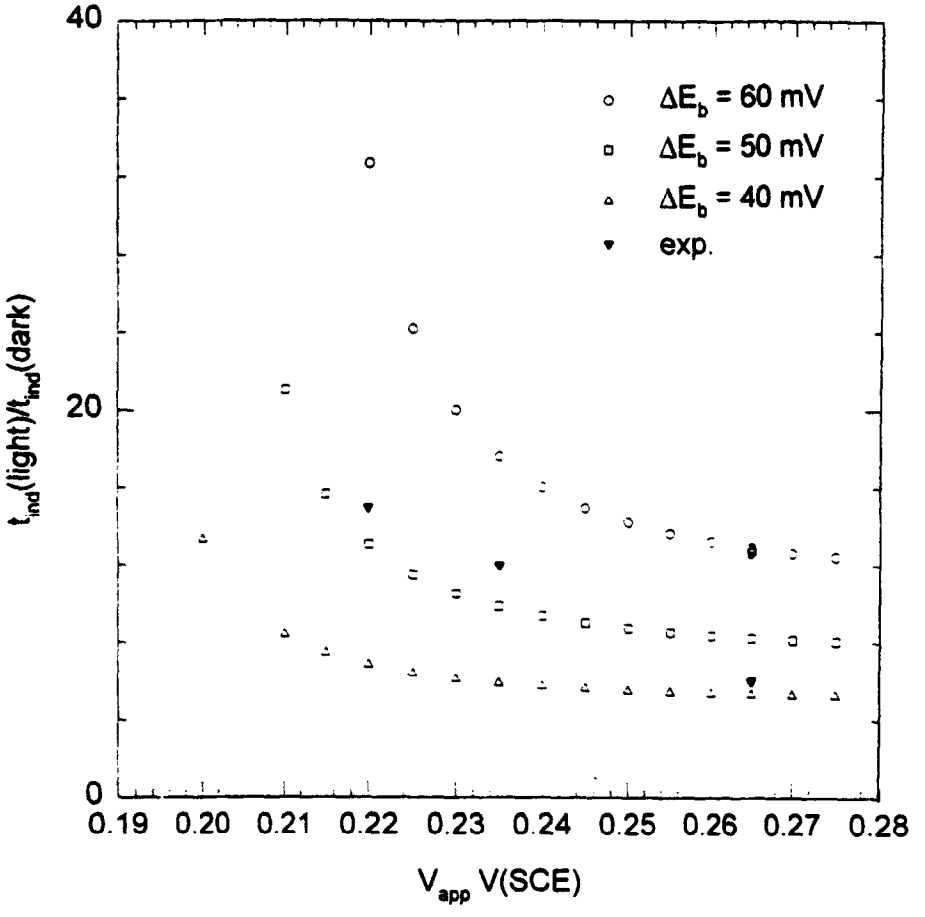

Fig. 8. Ratios of the induction periods for illuminated specimens and non-illuminated specimens, t^l_{ind}/t^d_{ind}, plotted as a function of the applied potential. Ratios calculated from experimental measurements: filled symbols. Ratios calculated using the Point Defect Model, allowing variations in the displacement of the critical breakdown potential, ΔE_b, on illumination: open symbols. The following values were used in calculations: $\alpha = 0.7$, $V^d_c = 150$ mV.

framework of the PDM and the semi-conducting nature of passive films. Nevertheless, the possibility of changes in the composition of the passive film on illumination, particularly an increase in the chromium to iron ratio, cannot be ruled out as this type of a process has been observed for a number of systems[30, 31].

CONCLUSIONS

It was found that illumination of Type 316 stainless steel with UV photons (300 nm, 400 μW cm^{-2}) leads to an increased resistance to the nucleation of pits in chloride solutions. This was evident from an increase in the breakdown potential, longer induction periods, and a significant decrease in the rate of pit nucleation once the induction periods elapsed. This increase in the resistance to pitting attack is explained in terms of the semiconducting nature of passive films and the Point Defect Model (PDM). It is proposed that the generation and separation of electron–hole pairs leads to a decrease in the electric field strength and a consequent modification of the vacancy structure. This in turn leads to a decrease in the flux of cation vacancies across the barrier layer, which results in an increased resistance to the nucleation of pits. Induction periods were measured under identical polarizing conditions for passive films formed in the light and in the dark. The experimentally-obtained ratios were then compared to the theoretical ratios calculated using the PDM. Good agreement between both sets of data was obtained supporting the proposed mechanism for the photo-inhibition effect.

ACKNOWLEDGEMENTS

The authors gratefully acknowledge the support of this work by the Electric Power Research Institute under Contract Number RP8041-07 and by the US Department of Energy/Basic Energy Sciences under Grant Number DE-F602-91ER45461.

REFERENCES

1. U. Stimming, *Electrochim. Acta* **31,** 415 (1986).
2. A. Di. Paola, F. Di. Quarto and C. Sunseri, *Corros. Sci.* **26,** 935 (1986).
3. T. D. Burleigh and R. M. Latanision, *J. Electrochem. Soc.* **134,** 135 (1987).
4. A. Di. Paola, D. Shukla and U. Stimming, *Electrochim. Acta.* **36,** 345 (1991).
5. S. M. Wilhelm and N. Hackerman, *J. Electrochem. Soc.* **123,** 1668 (1981).
6. M. J. Kloppers, F. Bellucci and R. M. Latanision, *Corrosion* **48,** 229 (1992).
7. A. K. Vijh, *Corros. Sci.* **12,** 105 (1972).
8. N. Sato, *J. Electrochem. Soc.* **128,** 225 (1982).
9. T. D. Burleigh and R. M. Latanision, *Corrosion* **432,** 471 (1987).
10. S. Menezes, R. Haak, G. Hogen and M. Kendig, *J. Electrochem. Soc.* **136,** 1884 (1989).
11. T. D. Burleigh, Corrosion **45,** 464 (1989).
12. G. Bianchi, A. Cerquetti, F. Massa and S. Torshio, *Localized Corrosion*, Vol. 3, p. 339. NACE, Houston (1974).
13. P. Schmuki and H. Böhni, *J. Electrochem. Soc.* **139,** 1908 (1992).
14. P. Schmuki and H. Böhni, *J. Electrochem. Soc.* **141,** 362 (1994).
15. S. J. Lenhart, M. Urquidi-Macdonald and D. D. Macdonald, *Electrochim. Acta.* **32,** 1739 (1987).
16. P. Schmuki and H. Böhni, *Proceedings of the Seventh International Symposium on Passivity of Metals and Semiconductors*, Clausthal-Zellerfeld, Germany, August 21–26 (1994).
17. P. Schmuki and H. Böhni, *Electrochim. Acta.* **40,** 775 (1995).
18. C. B. Breslin, D. D. Macdonald, E. Sikora and J. Sikora, *Electrochim. Acta.* **42,** 137 (1997).
19. E. Sikora, M. W. Balmas, D. D. Macdonald and R. C. Alkire, *Corros. Sci.* **38**(1), 97 (1996).
20. L. F. Lin, C. Y. Chao and D. D. Macdonald, *J. Electrochem. Soc.* **128,** 1194 (1981).
21. D. D. Macdonald, *J. Electrochem. Soc.* **139,** 3434 (1992).
22. T. Shibata, *Trans ISIJ* **23,** 785 (1983).
23. D. E. Williams, J. Stewart and P. H. Balkwill, *Corros. Sci.* **36,** 1213 (1994).
24. P. C. Pistorius and G. T. Burstein, *Corros, Sci.* **33,** 1885 (1992).
25. P. C. Pistorius and G. T. Burstein, *Corros. Sci.* **36,** 525 (1994).
26. D. D. Macdonald and D. Heaney, to be published.
27. A. Goossens, M. Vazquez and D. D. Macdonald, *Electrochim. Acta.* **41,** 47 (1996).
28. D. J. Ellerbrock and D. D. Macdonald, *Mat. Sci. Forum.* **927,** 185 (1995).
29. T. Haruna and D. D. Macdonald, *Scan Rate Dependence of the Pitting Potential on the Basis of the Point Defect Model*, Extended Abstracts, Electrochemical Society, Vol. 95-2, Abstr. 125, p. 209 (1995).
30. F. Mansfeld, S. H. Lin and L. Kwiatkowski, *Corrosion*, 50, 838 (1994).
31. C. Y. Lu, M. B. Ives, G. I. Sproule and M. J. Graham, H. H. Uhlig Memorial Symposium, The Electrochemical Society, Proc. Vol. 94–26, p. 151 (1994).